QUANTUM SIMULATION

Direct geometric probe of singularities in band structure

Charles D. Brown^{1,2,4}*, Shao-Wen Chang^{1,2}, Malte N. Schwarz^{1,2}, Tsz-Him Leung^{1,2}, Vladyslav Kozii^{1,3,5}, Alexander Avdoshkin¹, Joel E. Moore^{1,3}, Dan Stamper-Kurn^{1,2,3}*

A quantum system's energy landscape may have points where multiple energy surfaces are degenerate and that exhibit singular geometry of the wave function manifold, with major consequences for the system's properties. Ultracold atoms in optical lattices have been used to indirectly characterize such points in the band structure. We measured the non-Abelian transformation produced by transport directly through the singularities. We accelerated atoms along a quasi-momentum trajectory that enters, turns, and then exits the singularities at linear and quadratic band-touching points of a honeycomb lattice. Measurements after transport identified the topological winding numbers of these singularities to be 1 and 2, respectively. Our work introduces a distinct method for probing singularities that enables the study of non-Dirac singularities in ultracold-atom quantum simulators.

nergy surfaces are used to describe the structure and dynamics of quantum systems whose Hamiltonians contain one or more continuous parameters. Notable examples include band structure, which describes the motion of single particles within a crystal as a function of their quasi-momentum, and the potential energy surfaces that describe molecules as a function of their nuclear coordinates. Each point on an energy surface corresponds to an eigenenergy and an eigenstate of the physical system. Although the energies themselves are highly important for explaining material (1, 2) and chemical (3-6)properties, so too are the local geometry and global topology of the eigenstate manifolds.

The geometry of an eigenstate manifold can be revealed through transport of a quantum state along a smooth path of parameters that define the system's Hamiltonian. This transport is generally nonholonomic, meaning that the state generated by transport from an initial to a final point depends on the path along which the system was transported. Such transport has been explored mainly in the two limiting cases in which the energy spectrum of a system is either largely gapped (7, 8) or entirely gapless (9) along a closed loop in parameter space. In the former limit, the state-space geometry generates a Berry phase; in the latter, the nonholonomy generalizes to a Wilson loop operator that describes a path-dependent rotation within the degenerate subspace. In terms of $|u_{\bf q}^m\rangle$, the cell-periodic part of the Bloch wave function that describes a single particle, both types of dynamics derive from the Berry connection matrix, $A_{\bf q}^{nm}\equiv i\langle u_{\bf q}^n|\partial_{\bf q}|u_{\bf q}^m\rangle$, which expresses the local geometry of state space. Focusing on the case of band structure, n and m are band indices, and ${\bf q}$ is the quasi-momentum. In the gapped limit, the Berry phase is determined solely by one (Abelian) diagonal element of this matrix; in the gapless limit, off-diagonal elements enter, leading to non-Abelian state rotations (10).

In this work, we explored the nonholonomy of transport through a state space containing singular points of degeneracy. One example of such points, which we probed experimentally, is the Dirac points of degeneracy between the n=1 and n=2 bands of the two-dimensional honeycomb lattice, lying at the \mathbf{K} and \mathbf{K}' points of the Brillouin zone (Fig. 1). Away from these points, the energy gap between the touching bands grows linearly with quasimomentum. The singular state geometry around each linear band-touching point (LBTP) has

profound implications for the material properties of graphene—for example, related to Klein tunneling of electrons through potential barriers (11) and the appearance of a half-integer quantum Hall effect (12). The Dirac point of the honeycomb lattice has been explored also in ultracold-atom experiments (13), including interferometric measurements of the Berry phase produced along trajectories that circle the Dirac point (14) and direct mapping of the Bloch-state structure across the Brillouin zone (15–17).

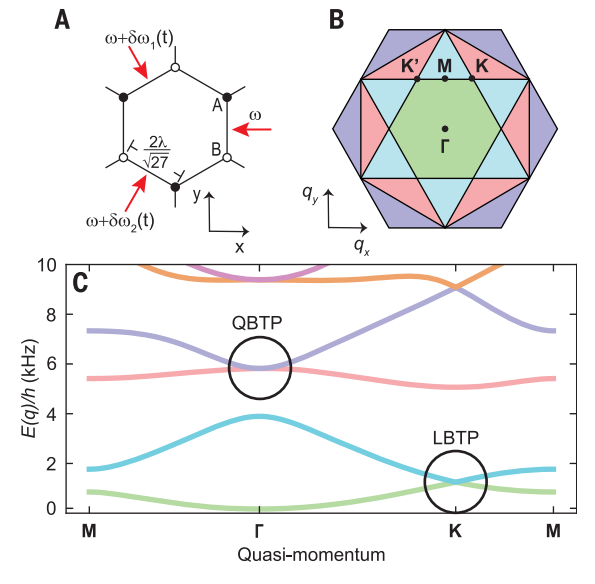
Crystalline materials may also host a singular quadratic band-touching point (QBTP), about which the energy gap between two bands grows quadratically with quasi-momentum. As before, the QBTP can profoundly affect material properties. For example, the singular QBTP is predicted to produce an anomalous Landau-level spectrum (18). Interactions can destabilize a QBTP, leading to topologically protected edge states, nematic phases, and both quantum anomalous Hall and spin phases (19-22). The role of QBTPs is being investigated intensely in both untwisted and twisted bilayer graphene (23-27). Despite their importance, QBTPs have remained unexplored in ultracold-atom systems.

Using ultracold atoms within an optical lattice, we demonstrated that transport of a quantum state through a singular band-touching point leads to a non-Abelian, coherent state rotation between bands, with the rotation depending on the relative orientation of path tangents entering and exiting the singular point. Further, we have shown that this dependence characterizes and distinguishes the Bloch-state geometry surrounding linear and quadratic band-touching singularities.

First, we considered the *s*-orbital LBTP of a two-dimensional honeycomb optical lattice (Fig. 1). To probe this Dirac point, we prepared

Fig. 1. Experimental scheme.

(A) Illustration of an optical honeycomb lattice with two sites ("A" and "B") in the unit cell, formed by overlapping three λ = 1064-nm wavelength light beams (red arrows). Offsetting the optical frequencies of two lattice beams by $\delta\omega_{1,2}(t)$ accelerates the lattice and drives lattice-trapped atoms through a trajectory in quasimomentum. (**B**) The $n = \{1, 2, 3, 4\}$ Brillouin zones of the honeycomb lattice are shown in green, blue, pink, and purple, respectively. (C) The band structure of the honeycomb lattice (plotted with potential depth of 20 kHz \times h) exhibits an LBTP in the s-orbital band manifold at q = K and a QBTP in the p-orbital band manifold at $\mathbf{q} = \mathbf{\Gamma}$.



¹Department of Physics, University of California, Berkeley, Berkeley, CA 94720, USA. ²Challenge Institute for Quantum Computation, University of California, Berkeley, Berkeley, CA 94720, USA. ³Materials Sciences Division, Lawrence Berkeley National Laboratory, Berkeley, CA 94720, USA. ⁴Department of Physics, Yale University, New Haven, CT 06520, USA. ⁵Department of Physics, Carnegie Mellon University, Pittsburgh, PA 15213, USA.

^{*}Corresponding author. Email: charles.d.brown@yale.edu (C.D.B.); dmsk@berkeley.edu (D.S.-K.)

an optically trapped ⁸⁷Rb Bose-Einstein condensate and then slowly ramped up an overlain static honeycomb lattice, placing the atoms initially at the Γ -point of the n=1 band. Next, we applied a fictitious force to the gas by accelerating the optical lattice potential to a velocity $\mathbf{v}_{\text{lat}}(t)$. Although the atoms remained at zero quasi-momentum in the laboratory frame, they evolved to nonzero velocity $\mathbf{v} = h\mathbf{q}/m = -\mathbf{v}_{\text{lat}}$ in the lattice frame, where h is Planck's constant h divided by 2π , \mathbf{q} is the lattice-frame quasi-momentum, and m is the atomic mass.

To demonstrate the nonholonomy generated by the LBTP, we accelerated the atoms on a trajectory that proceeded at constant acceleration from Γ to \mathbf{K} (at quasi-momentum $\mathbf{q}_{\mathbf{K}}$) and then at a different constant acceleration to 24 distinct points on a circle lying at a distance of $0.4\|\mathbf{q_K}\|$ from the **K**-point. The turning angle between the rays entering and leaving the K-point, as defined in Fig. 2A, was varied in equal steps over $\theta \in [0, 2\pi]$. We then performed "band mapping" by smoothly ramping off the lattice potential at the fixed final quasi-momentum-that is, with the lattice at a constant final laboratory-frame velocity. This ramp maps the population in each band onto a distinct momentum state. Measuring this momentum distribution quantified band populations in the moving lattice.

Transport along paths passing through the singular LBTP led to interband transitions that varied with the turning angle (Figs. 2, C and D). For trajectories that entered the singularity and then reversed onto themselves $(\theta = 0)$, the population remained nearly entirely in the initial n = 1 band. For trajectories that continued with constant tangent through the singularity $(\theta = \pi)$, the atoms underwent a near complete transition to the upper n = 2 bands [seen also in (28)]. Over the full range of θ , each population underwent one cycle of oscillation.

The unit-cell wave function of the n = 1 and n = 2 Bloch states near the Dirac point can be represented as a pseudo-spin-1/2 vector, with s-orbital Wannier states at the lattice sites A and B representing the up- and down-spin basis states. In this basis, the Bloch states are eigenstates of the Hamiltonian H_{LBTP} = $-\mathbf{B}(\mathbf{q})\cdot\boldsymbol{\sigma}$, where $\mathbf{B}(\mathbf{q})$ is a pseudo-magnetic field that lies in the transverse pseudo-spin plane, and σ is the vector of Pauli matrices. **B**(\mathbf{q}) has a magnitude $B = \hbar v_g \|\mathbf{q} - \mathbf{q_K}\|$ that varies linearly with distance from the singularity and has an orientation (in the proper gauge) that is radially outward from **K** (Fig. 2B). Here, v_{g} is the group velocity near the Dirac point. The 2π rotation of $\mathbf{B}(\mathbf{q})$ about the Dirac point is responsible for the π -valued Berry phase of trajectories that encircle the Dirac point (14).

This pseudo-spin model explains our observations. The atomic pseudo-spin entering the

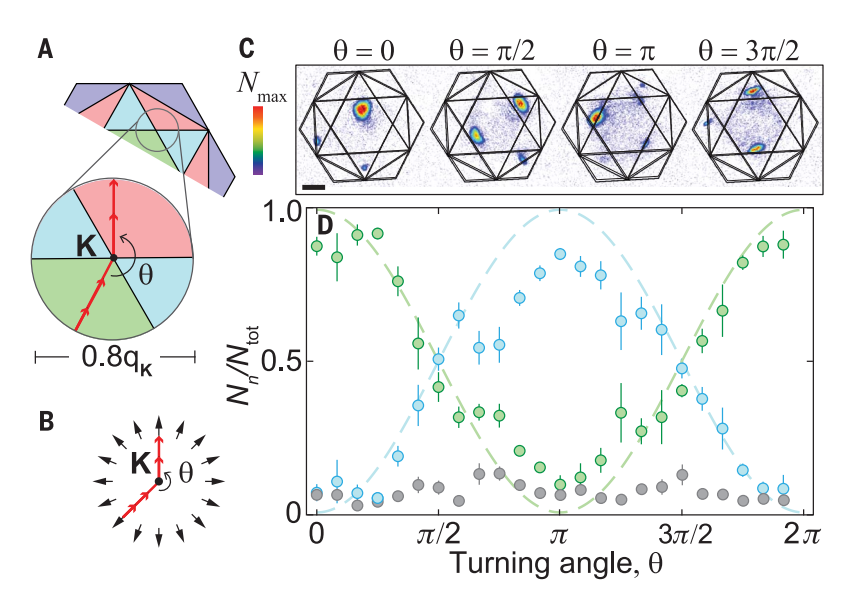


Fig. 2. Non-Abelian state rotations around a Dirac point. (**A**) Enlarged view of Brillouin zone map. Atoms are loaded into the state n=1, $\mathbf{q}=\Gamma$ in the lattice and transported (trajectory indicated with red arrows) at constant accelerations from $\Gamma \to \mathbf{K}$ and then from **K** to a final point lying on a circle of diameter $0.8\|\mathbf{q_K}\|$ centered at the Dirac point. In this particular experiment, the atoms evolve between the n=1 and n=2 bands. The colors of the Brillouin zones do not indicate the state of the atomic wave packet along the trajectory. Rather, the color scheme is used to interpret the band index of atoms after a band-mapping measurement. (**B**) Bloch states near the Dirac point are described as pseudo-spin-1/2 states in a pseudo-magnetic field (black arrows) that points radially outward from, and wraps once around, the Dirac point. (**C**) Band-mapping images at the final quasi-momentum, with overlain Brillouin zone maps, show that the band populations vary with turning angle θ. A third, short-length, and adiabatic translation step ensures that band mapping does not occur near a Brillouin zone boundary so that there is no ambiguity in the band index of atoms [(31), section 3]. Scale bar, 0.1 mm. (**D**) Fractional band populations N_n/N_{total} (n=1, green; n=2, blue; sum of other bands, gray) versus θ. Means and standard mean errors are determined from seven repeated measurements. The green and blue dashed lines indicate a $\cos^2(\theta/2)$ and $\sin^2(\theta/2)$ dependence, respectively.

Dirac point along a ray experiences a pseudomagnetic field whose orientation \mathbf{n} remains constant and whose magnitude smoothly tunes to zero. Under this field, the initial-state pseudospin remains aligned along **n**. Departing the Dirac point, the pseudo-spin experiences a magnetic field along a new orientation m, with $\mathbf{n} \cdot \mathbf{m} = \cos \theta$, and a magnitude increasing linearly with time. The pseudo-spin is thus placed in a superposition of eigenstates, with population $\cos^2(\theta/2)$ in the **m**-oriented pseudospin eigenstate (n = 1 bands) and $\sin^2(\theta/2)$ in the orthogonal state (n = 2 bands). This simple prediction is in good agreement with our data (Fig. 2D), with residual differences accounted by numerical simulations (fig. S6) of the dynamics of noninteracting atoms over the finite duration of our experimental stages (29).

We found that passage through the Dirac point produces a phase-coherent superposition of band states. Such coherence was demonstrated by allowing the atoms to evolve at the final point of the trajectory for a variable time before measuring populations in a basis different from the local energy eigenbasis. Temporal oscillations in these measurements, with a frequency matching the calculated gap between the

n = 1 and n = 2 bands, demonstrate the coherence of the atomic state after transport (fig. S3).

The energy-time uncertainty relation places a bound on how finely the singular point can be located by our method. We considered a trajectory where the acceleration has magnitude a near the singularity. The system spends a time $\delta t \sim (\hbar/ma)\delta q$ within δq of the singularity; the energy gap has magnitude $\delta E \sim \hbar v_{\rm g} \delta q$ in that vicinity. Setting $(\delta t)(\delta E) \sim \hbar$ establishes that the band structure is effectively gapless within a quasi-momentum distance of $\delta q = R \sim \sqrt{ma\hbar/v_{\rm g}}$ of the singularity. That is, the nonholonomy generated by the singular point should be observed also for finite time trajectories that pass within the effective radius, R, of the singularity.

We measured R by driving the atoms along a family of trajectories (Fig. 3A) that connect between the initial Γ -point to a final Γ -point that is one reciprocal lattice vector away, and by performing band-mapping measurements at the final point. These trajectories cross the boundary between the first and second Brillouin zones at nine equally spaced points along the $\mathbf{K'} - \mathbf{M} - \mathbf{K}$ line. As shown in Fig. 3B for various traversal times τ , we observed that

trajectories that pass directly through either Dirac point yield a band population distribution that is independent of τ , with ~3/4 of the atoms transferring to the upper band. By contrast, for traversal times that are longer and for paths that veer farther from the Dirac points, the transition between bands is increasingly suppressed, demonstrating that R decreases with decreasing a (increasing τ). At first glance, the experiment of Fig. 3 is analogous to Majorana losses. The study presented in Fig. 3 is quite close to Majorana's description (30) and to the picture of the "Majorana hole" that appears in a spherical quadrupole magnetic trap. However, a difference between our experiment and magnetic traps is that in traps, the spin flips that occur because of transport through the state geometry of the system lead to loss, whereas in our experiment, they led to transitions between trapped bands of the lattice.

The singularity at an LBTP can be characterized by two different experimental methods: either by Berry phase measurements along trajectories that encircle the singularity (14), or as shown here, through state rotations produced along trajectories that pass through the singularity. These two methods are related but nonequivalent. Berry phase measurements measure the integrated Berry flux, which is determined from a diagonal element of the Berry connection matrix $A_{\mathbf{q}}^{nn}$. A π -valued flux was found pinned to the singular point. By contrast, the non-Abelian state rotations detected in our method derived directly from the off-diagonal elements $A_{\mathbf{q}}^{nm}$, with n = 1 and m = 2 being the two crossing bands (31). Further, different from Berry phase measurements, our method can be regarded as measuring the Hilbert-Schmidt quantum distance $d^2(\mathbf{q},\mathbf{q}')=1-\left|\left\langle u^1_{\mathbf{q}'} | u^1_{\mathbf{q}} \right\rangle\right|^2$ (32, 33), with **q** identified as a point along the input path into, and q' as a point along the exit path from, the singularity. The oscillation of the n = 1 band population as a function of the turning angle reveals the quantum distance to undergo one complete oscillation between zero and unity on a contour encircling the LBTP.

The distinction between these two methods is notable in the case of a QBTP. Similar to the LBTP, a singular QBTP also carries concentrated Berry flux that is restricted, assuming time reversal and C_6 symmetry, to be 0 or $\pm 2\pi$ (20). However, these values of Berry phase are undetectable with interference measurements. By contrast, our method uncovers the characteristic nonholonomy of the singular QBTP and the concomitant modulation of the quantum distance around the singular point.

For a singular QBTP, the geometric structure of Bloch states of the two intersecting bands at the vicinity of the singularity can again be described as those of a pseudo-spin in a pseudo-magnetic field. Different from the LBTP, in this work the pseudo-magnetic field, lying in the transverse pseudo-spin plane, has a magnitude that increases quadratically with distance to the singularity and has an orientation that wraps by an angle of 4π along a path encircling the singularity (Fig. 4B).

We probed this geometric structure at the QBTP that occurs at Γ between the n=3 and n = 4 bands of the honeycomb lattice. For this, we first loaded the Bose-Einstein condensate into the n = 3 bands of the lattice by means of "inverse band mapping." In previous work (34), such loading into excited bands was realized with moving atoms in a static lattice; in this study, we realized similar state-preparation with static atoms loaded into a moving lattice. Specifically, we gradually increased the depth of a honeycomb lattice moving with velocity $\mathbf{v}_{\mathbf{Q}}$ that is located within the third Brillouin zone in the extended zone scheme (Fig. 4A). Then, we accelerated atoms (in the lattice frame) at constant acceleration along the path $\mathbf{Q} \rightarrow \Gamma$, into the QBTP, and then turning by an angle θ , accelerated the atoms at a different constant acceleration out of the QBTP and to the edge of the Brillouin zone. Final points were chosen as ones where populations in the n = 3 and n = 4 bands were easily distinguished with band mapping.

Fig. 3. Effective size of a Dirac singularity.

(A) Illustration of quasi-momentum trajectories over which the atoms are transported for the measurements in (B). Each trajectory connects two different Γ -points but traverses one of nine equally spaced points along the K' - M - K line. (**B**) Fractional n = 1 band population plotted, for different trajectory traversal times τ , against the trajectory midpoints from (A). Means and standard mean errors are generated from three to five repeated measurements. (C) An effective radius R (plotted normalized by $\hbar k = h/\lambda$) is defined for each τ by the distance along the $\mathbf{K'}$ - \mathbf{M} - \mathbf{K} line for which the threshold $N_1/N_{total} = 0.5$ is fulfilled. R diminishes with larger τ.

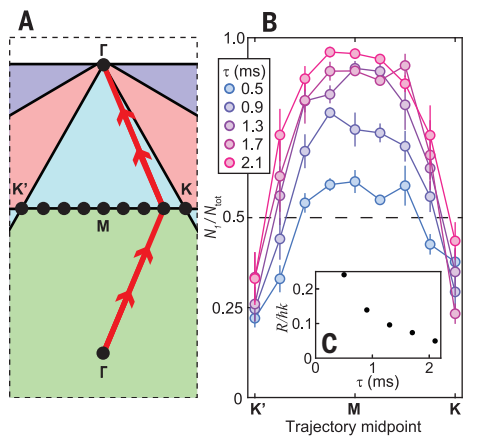
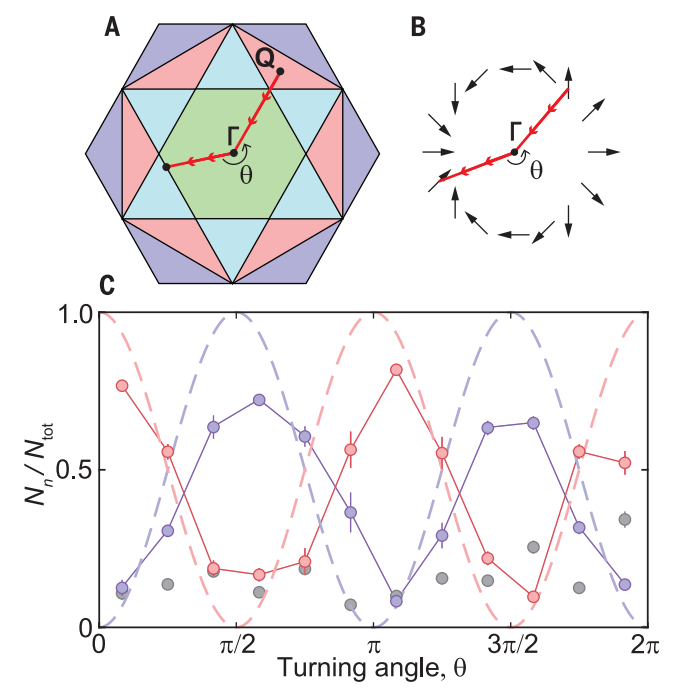


Fig. 4. Non-Abelian state rotations around a QBTP.

(A) Atoms are prepared in the n = 3 bands at \mathbf{Q} , transported (along red arrows) to the QBTP at Γ , and then transported to a final quasi-momentum for band mapping. In this particular experiment, the atoms evolve between the n = 3 and n = 4 bands. The colors of the Brillouin zones do not indicate the state of the atomic wave packet along the trajectory. Rather, the color scheme is used to interpret the band index of atoms after a band-mapping measurement. (B) The pseudo-magnetic field (black arrows) describing the Bloch state geometry wraps

twice in orientation for one revolution around the QBTP.



(C) A plot of normalized band population as a function of θ , collected by analyzing band-mapping data (fig. S2). Red circles indicate the n = 3 bands; purple circles indicate the n = 4 band; and gray circles indicate bands with $n \neq 3$, 4. Mean and standard mean errors are determined from seven repeated measurements. The dashed pink and purple lines indicate a $\cos^2(\theta)$ and $\sin^2(\theta)$ dependence, respectively. Our numerical simulations suggest that the data does not reach unity oscillation amplitude owing to nonadiabaticity in the band-mapping procedure (fig. S6).

We observed a nonholonomy at the QBTP that was distinct from that observed at the LBTP. Specifically, we observed two cycles of oscillation in the final band populations over the interval $\theta \in [0, 2\pi]$. This behavior is explained well by the pseudo-spin representation of the singular QBTP. Different from the LBTP, pseudo-magnetic-field orientations along the incoming (**n**) and outgoing (**m**) paths were related as $\mathbf{n} \cdot \mathbf{m} = \cos 2\theta$. The nonholonomy of the QBTP produced populations of $\cos^2(\theta)$ and $\sin^2(\theta)$ in the n=3 (initial) and n=4 bands, respectively.

The amplitude of the observed oscillation is lower than suggested by this simple theory; again, we ascribe this difference to dynamical effects of our finite-duration acceleration and band-mapping stages. Nevertheless, the periodicity of the oscillations, combined with the known time reversal and C_6 symmetry of our lattice, unambiguously determined the topological winding number around the QBTP to be well defined and equal to 2 (31).

We have demonstrated transport of a quantum system through singular band-touching points with different topological winding numbers. We observed non-Abelian, coherent state rotation between bands. The dependence of this rotation on the relative orientation of path tangents entering and exiting the singular point unambiguously measured the winding number.

Our method of probing band structure could be applied to gain insight on other band structure singularities and on interaction effects. It would be interesting to study higher-order singular band-touching points, between more than two bands. We deliberately minimized interaction effects in these experiments, but in future work, it will be interesting to observe potential interaction-induced instabilities of Dirac points, QBTPs, or other band-touching points. The path-dependent non-Abelian non-holonomy observed in this work may also pertain to chemical systems, in which potential energy surfaces are endowed similarly with conical intersections (3–6), suggesting a potential route for quantum state control in optically driven molecules.

REFERENCES AND NOTES

- D. Xiao, M.-C. Chang, Q. Niu, Rev. Mod. Phys. 82, 1959–2007 (2010).
- A. Bansil, H. Lin, T. Das, Rev. Mod. Phys. 88, 021004 (2016).
- D. R. Yarkony, J. Phys. Chem. A 105, 6277–6293 (2001).
- G. A. Worth, L. S. Cederbaum, Annu. Rev. Phys. Chem. 55, 127–158 (2004).
- W. Domcke, D. R. Yarkony, Annu. Rev. Phys. Chem. 63, 325–352 (2012).
- M. S. Schuurman, A. Stolow, Annu. Rev. Phys. Chem. 69, 427–450 (2018)
- 7. B. Simon, Phys. Rev. Lett. 51, 2167-2170 (1983).
- M. V. Berry, Proc. R. Soc. London Ser. A 392, 45–57 (1984).
 F. Wilczek, A. Zee, Phys. Rev. Lett. 52, 2111–2114 (1984).
- A. Bohm, A. Mostafazadeh, H. Koizumi, Q. Niu, J. Zwanziger, The Geometric Phase in Quantum Systems (Springer, 2003).
- M. I. Katsnelson, K. S. Novoselov, A. K. Geim, *Nat. Phys.* 2, 620–625 (2006).
- Y. Zhang, Y.-W. Tan, H. L. Stormer, P. Kim, *Nature* 438, 201–204 (2005).
- L. Tarruell, D. Greif, T. Uehlinger, G. Jotzu, T. Esslinger, *Nature* 483, 302–305 (2012).
- 14. L. Duca et al., Science 347, 288-292 (2015).
- 15. M. Tarnowski et al., Phys. Rev. Lett. 118, 240403 (2017).
- 16. T. Li et al., Science 352, 1094-1097 (2016)
- 17. N. Fläschner et al., Science 352, 1091-1094 (2016).
- J.-W. Rhim, K. Kim, B.-J. Yang, Nature 584, 59–63 (2020).
 K. Sun, E. Fradkin, Phys. Rev. B Condens. Matter Mater. Phys. 78, 245122 (2008).
- K. Sun, H. Yao, E. Fradkin, S. A. Kivelson, *Phys. Rev. Lett.* 103, 046811 (2009).
- J. M. Murray, O. Vafek, Phys. Rev. B Condens. Matter Mater. Phys. 89, 201110 (2014).
- 22. J. Shah, S. Mukerjee, *Phys. Rev. B* **103**, 195118 (2021).
- 23. E. McCann, V. I. Fal'ko, *Phys. Rev. Lett.* **96**, 086805
- E. McCann, M. Koshino, Rep. Prog. Phys. 76, 056503 (2013).
- S. Pujari, T. C. Lang, G. Murthy, R. K. Kaul, *Phys. Rev. Lett.* 117, 086404 (2016).
- 26. K. Hejazi, C. Liu, L. Balents, Phys. Rev. B 100, 035115 (2019).
- K. Hejazi, C. Liu, H. Shapourian, X. Chen, L. Balents, *Phys. Rev. B* 99, 035111 (2019).

- 28. G. Jotzu et al., Nature 515, 237-240 (2014).
- 29. The maximum duration of our experiment was limited by the observed decay of atoms from the excited-energy Bloch states populated during lattice acceleration.
- 30. E. Majorana, Nuovo Cim. 9, 43-50 (1932).
- Materials and methods are available as supplementary materials.
- 32. J. P. Provost, G. Vallee, Commun. Math. Phys. **76**, 289–301 (1980).
- Y. Hwang, J. Jung, J.-W. Rhim, B.-J. Yang, *Phys. Rev. B* 103, L241102 (2021).
- 34. T.-H. Leung et al., Phys. Rev. Lett. 125, 133001 (2020).
- 35. C. D. Brown et al., Dataset for direct geometric probe of singularities in band structure. Zenodo (2022).

ACKNOWLEDGMENTS

We thank E. Altman, M. Zaletel, N. Read, and J. Harris for early insights into this work. Funding: We acknowledge support from the NSF QLCI program through grant OMA-2016245 and also NSF grant PHY-1806362, and from the ARO through the MURI program (grant W911NF-17-1-0323). C.D.B. acknowledges support from the National Academies of Science, Engineering, and Medicine Ford Postdoctoral Fellowship program. V.K. and J.E.M. were supported by the Quantum Materials program at LBNL, funded by the US Department of Energy under contract DE-AC02-05CH11231. A.A. and J.E.M. acknowledge support from the NSF under grant DMR-1918065 and from a Kavli ENSI fellowship. J.E.M. acknowledges support from a Simons Investigatorship. Author contributions: All authors contributed substantially to the work presented in this manuscript, C.D.B., S.-W.C., M.N.S. and T.-H.L. acquired the data and maintained the experimental apparatus. C.D.B., S.-W.C., and M.N.S. analyzed the data. C.D.B. prepared the manuscript. M.N.S. A.A., and V.K. performed the numerical calculations. A.A. and V.K. performed supporting theory calculations. J.E.M. and D.S.-K. supervised the study. All authors worked on the interpretation of the data and contributed to the final manuscript. Competing interests: The authors declare no competing interests. Data and materials availability: The data and the codes used for both data analysis and theory curve generation are available at Zenodo (35). License information: Copyright © 2022 the authors, some rights reserved; exclusive licensee American Association for the Advancement of Science. No claim to original US government works. https://www.science.org/about/sciencelicenses-journal-article-reuse

SUPPLEMENTARY MATERIALS

science.org/doi/10.1126/science.abm6442 Materials and Methods Supplementary Text Figs. S1 to S7 References (36–41)

Submitted 4 October 2021; accepted 28 July 2022 10.1126/science.abm6442



Direct geometric probe of singularities in band structure

Charles D. Brown, Shao-Wen Chang, Malte N. Schwarz, Tsz-Him Leung, Vladyslav Kozii, Alexander Avdoshkin, Joel E. Moore, and Dan Stamper-Kurn

Science, 377 (6612), .

DOI: 10.1126/science.abm6442

Zooming through singularities

Singularities in the band structure of materials often have a profound influence on their properties. Like the better-known Dirac points, in which linearly dispersing bands touch, quadratic band-touching points can lead to exotic effects. Brown *et al.* introduce a method of studying both of these types of singularities in a cold atom quantum system. In their experiment, atoms of rubidium-87 were placed in a honeycomb optical lattice and driven through the singularities along various trajectories by accelerating the lattice potential. By measuring the band population, the researchers were able to determine the winding number of the singularities. —JS

View the article online

https://www.science.org/doi/10.1126/science.abm6442

Permissions

https://www.science.org/help/reprints-and-permissions

Use of this article is subject to the Terms of service